Tracked 3D Ultrasound Targeting with an Active Cannula

Philip J. Swaney[1]*, Jessica Burgner[1], Thomas S. Pheiffer[2], D. Caleb Rucker[1], Hunter B. Gilbert[1], Janet E. Ondrake[2], Amber L. Simpson[2], E. Clif Burdette[3], Michael I. Miga[2], and Robert J. Webster III[1]

[1]Department of Mechanical Engineering, Vanderbilt University, Nashville, Tennessee, U.S.A.;
[2]Department of Biomedical Engineering, Vanderbilt University, Nashville, Tennessee, U.S.A.;
[3]Acoustic MedSystems, Inc., Champaign, Illinois, U.S.A.

ABSTRACT

The objective of our work is a system that enables both mechanically and electronically shapable thermal energy deposition in soft tissue ablation. The overall goal is a system that can percutaneously (and through a single organ surface puncture) treat tumors that are large, multiple, geometrically complex, or located too close to vital structures for traditional resection. This paper focuses on mechanical steering and image guidance aspects of the project. Mechanical steering is accomplished using an active cannula that enables repositioning of the ablator tip without complete retraction. We describe experiments designed to evaluate targeting accuracy of the active cannula (also known as a concentric tube robot) in soft tissues under tracked 3D ultrasound guidance.

Keywords: Steerable Needle, Liver, Ablation, Ultrasound, Robotic Surgery, Image-Guided Surgery, Image-Guided Therapy

1. INTRODUCTION

Needles are vital tools in medicine that enable minimally invasive access to the body for diagnostic procedures like biopsy, and interventional procedures like brachytherapy, injection, thermal therapy, etc. Accurately placing the needle tip at the clinically-desired location is essential to the success of these procedures. It has been well-established by many researchers that robots can effectively assist physicians with the task of placing a needle tip at a desired location specified on a medical image[1] and that needles can be "steered" through curved trajectories in tissue[2]. It has also been shown that needle alignment can be improved by image-guidance robotic devices, in comparison with traditional manual needle insertion by the physician[3].

Most prior needle insertion systems insert straight needles. In these systems the objective is simply to align the needle with the desired trajectory before insertion begins. While these systems are adequate for many types of surgical intervention, they have two drawbacks. First, they do not provide a means to compensate for unmodeled effects during insertion (e.g. needle deformation, tissue deformation, etc.), as well as residual calibration and registration errors (which are usually small, but often remain non-negligible). Second, there are some locations that are obscured by obstacles (bones, blood vessels, nerves, etc.) making straight-line trajectories infeasible or more invasive than curved paths. An example is that the pubic arch can obstruct parts of the prostrate during brachytherapy in some cases. These factors have inspired steerable needles.

A variety of different needle steering methods have been proposed over the past few years. One of the first concepts was applying lateral forces and moments during insertion at the base of a standard straight needle[4,5]. A flexible needle can also be directed using a bevel tip through a curved trajectory (that is "steered") by controlling the axial rotation of the needle shaft during insertion[6,7]. It is also possible to use a "catheter-like" approach, where a pre-bent stylet is extended from a straight outer tube[8]. A different approach which does not rely as heavily on needle-tissue interaction forces is to use multiple precurved concentric tubes, which can each be translated and rotated with respect to one another at their respective bases[9,10,11,12]. By using the elastic interaction between the tubes, this active cannula (also referred to as a concentric tube robot – the terms are interchangable) is able to "steer" through free space as well as when embedded in soft tissue.

*Corresponding Author. Email: philip.j.swaney(at)vanderbilt.edu

In this paper, we present some initial steps toward the overall goal of using an active cannula to deploy an acoustic ablation probe to treat liver cancer. There are over one million new cases worldwide per year of hepatocellular carcinoma, the most frequently occurring type of primary liver cancer[13]. It is also common for cancer to metastasize from other locations to the liver. In 2005, there were 73,000 cases of primary colon cancer metastasizing to the liver in the United States alone[14]. It has been shown that radiofrequency ablation is a useful treatment method for hepatic tumors[15]. However, current ablation systems cannot treat large, multiple, or oddly shaped tumors through a single insertion, due to limited control of the shape and size of the thermal treatment zone. To provide a means of treating these types of tumors through a single insertion point (which significantly reduces liver trauma), Burdette, et al. proposed a system that can re-deploy an ablator to multiple locations inside the liver without retracting it, using an active cannula[16]. The ablator used is an ultrasonic interstitial thermal therapy (USITT) probe, which has the highly useful properties of (1) providing an electronically shapable ablation zone, (2) using a form of energy (mechanical waves) that propagates deeper into tissue than alternative ablation technologies, enabling larger ablation zones, and (3) creating solid and consistent coagulation throughout the tumor without charring or vaporization[17,18].

In this paper, we extend the initial work of Burdette, et al. in several important ways. First, we use a robot to deploy the device rather than a passive device with manual control knobs. Second, we present a new method for simultaneous registration and calibration of the robot and the tracked ultrasound probe used to guide it. Lastly, we present experimental results with the system, delivering the tip of the ablator to the physical coordinates of desired ultrasound image points. These experiments are conducted in free space, phantom tissue, and ex-vivo liver.

2. EXPERIMENTAL SETUP

A concentric tube robot (see Figure 1a) is made of several telescoping pre-curved superelastic tubes. Each tube is grasped at its base, where it is rotated and translated with respect to the other tubes. This is accomplished using the robotic actuation unit shown in Figure 1, which was designed to deliver an Ultrasonic Interstitial Thermal Therapy (USIT) ablator[16]. The unit is modular, allowing for extra carriers and tubes to be added based on the desired cannula workspace.

Each tube is controlled by one carrier. A carrier translates itself (and thereby its tube) linearly along a fixed lead screw as a motor in the carrier spins a nut that interfaces with the lead screw. Tube axial rotation is achieved by a second motor in the carrier that rotates a worm gear, which interfaces with a gear attached to the tube, creating a non-backdrivable design. Low level control of two motors on each carrier is implemented using a Galil DMC-4080 (Galil Motion Control, USA). A nitinol tube was heat treated to create the inner tube with a 196 mm radius of curvature. The outer tube was a straight, stiff, stainless steel tube. Our active cannula was outfitted with a simulated ablator consisting of a small thermoplastic tip matching the geometry of the USITT ablator tip.

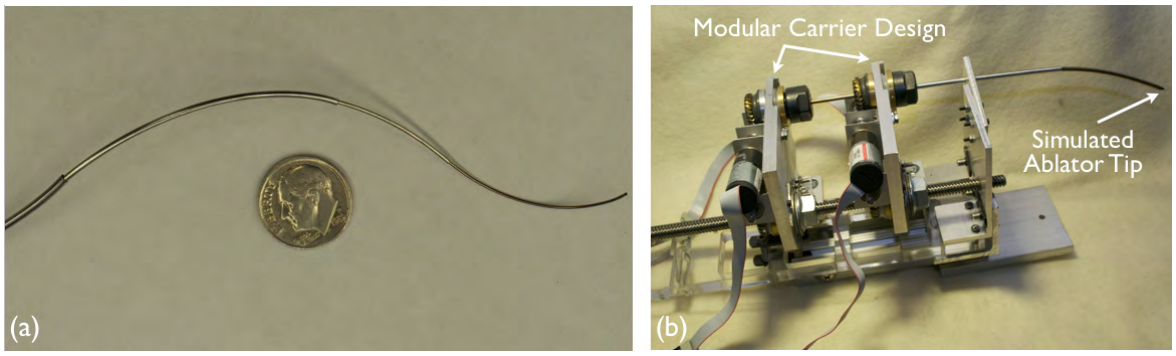

Figure 1. (a) A four-tube concentric robot. (b) Photograph of the robotic actuation unit used to control the active cannula tubes in our experiment. The device has a small footprint of 48 × 12 × 12 cm. As pictured it can actuate two tubes. The design is modular, making it straightforward to add more carriers and hence more tubes.

The ultrasound machine used in this study was a Siemens ACUSON Antares system (Siemens Medical Solutions USA, Inc.) with a VFX9-4 linear array transducer (4-9 MHz). The tracking system used was a NDI Hybrid Polaris Spectra optical tracker (Northern Digital, Inc., Canada), which is reported by NDI as having a RMSE of 0.35 mm. In order to track the position and orientation of ultrasound images, an optical tracking marker was affixed to the ultrasound transducer, as shown in Figure 2.

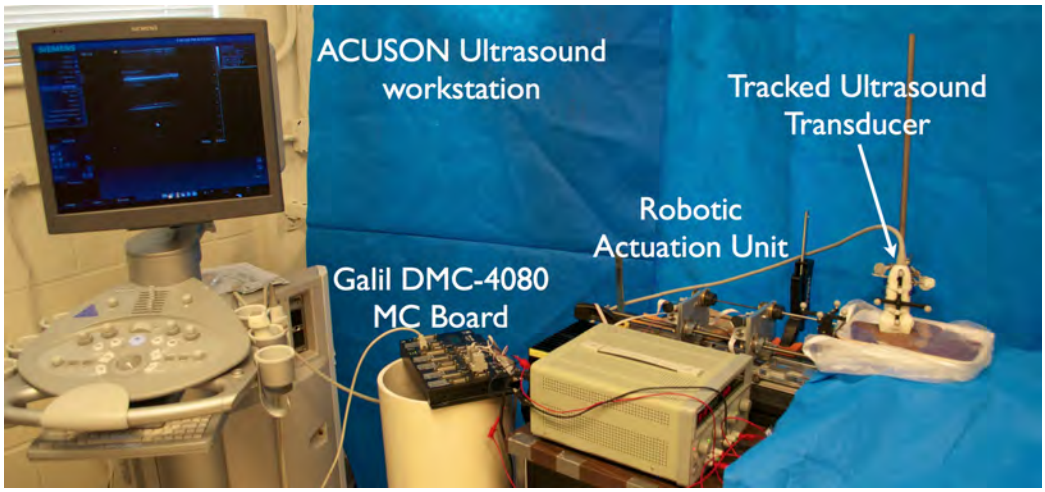

Figure 2. Tracked robotic actuation unit and ultrasound probe with workstation used for targeting experiments.

2.1 Active Cannula Kinematics

In order to determine the Cartesian location of the USITT tip for a given configuration of actuator values, several constants must be defined as shown in Figure 3. These kinematic equations were derived in Burdette, et al.[16] and are given here for completeness. The total length of each tube (L_1, L_2, L_3) and the translational distances between the tube bases and the robot frame origin at the front plate (D_1, D_2, D_3) are then used to calculate the combined tube curvature (κ_1) and the segment lengths (ℓ_1, ℓ_2, ℓ_3) as follows,

$$\begin{aligned}
\kappa_1 &= \frac{E_2 I_2}{E_1 I_1 + E_2 I_2} \kappa_2 \\
\ell_1 &= L_1 - D_1 \\
\ell_2 &= L_2 - D_2 - \ell_1 \\
\ell_3 &= L_3 - D_3 - \ell_1 - \ell_2
\end{aligned}$$

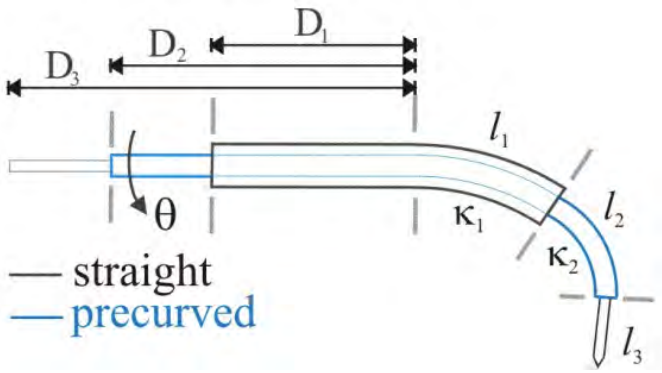

Figure 3. Sketch showing the variable definitions used for active cannula kinematics.

Here, E_i and I_i are the Young's Modulus of tube i and cross sectional moment of inertia respectively. The segment ℓ_1 is the length of the curved portion of the inner and outer tube combination measured from the front plate to the tip of the outer tube. Segment ℓ_2 is the length of the curved portion of the inner tube extending from the outer tube, measured from the tip of the outer tube to the tip of the inner tube (see Figure 3). The segment ℓ_3 is the distance the ablator tip is extended from the tip of the inner tube. κ_2 is the curvature of the precurved portion of the inner tube, and κ_1 is the curvature of the first segment ℓ_1 (i.e. the curvature of the inner and outer tube combination). Using these values and the rotation angle of the inner tube θ, the Cartesian location of the tip is given by,

$$x = \frac{1}{\kappa_1\kappa_2}(\kappa_1 \cos(\ell_1\kappa_1 + \ell_2\kappa_2) - \kappa_2 - \ell_3\kappa_1\kappa_2 \sin(\ell_1\kappa_1 + \ell_2\kappa_2) + (\kappa_2 - \kappa_1)\cos(\ell_1\kappa_1))\cos\theta$$
$$y = \frac{1}{\kappa_1\kappa_2}(\kappa_1 \cos(\ell_1\kappa_1 + \ell_2\kappa_2) - \kappa_2 - \ell_3\kappa_1\kappa_2 \sin(\ell_1\kappa_1 + \ell_2\kappa_2) + (\kappa_2 - \kappa_1)\cos(\ell_1\kappa_1))\sin\theta$$
$$z = \frac{1}{\kappa_1\kappa_2}(\kappa_1 \sin(\ell_1\kappa_1 + \ell_2\kappa_2) + \ell_3\kappa_1\kappa_2 \cos(\ell_1\kappa_1 + \ell_2\kappa_2) + (\kappa_2 - \kappa_1)\sin(\ell_1\kappa_1))$$

2.2 Inverse Kinematics

Given a desired target (x, y, z) we wish to determine actuator values D_1, D_2, D_3, and θ for a target tip location. In this paper, a fixed value for ℓ_3 was used, reducing the configuration variables to D_1, D_2, and θ. The actuator values were determined by numerically solving the above system of nonlinear equations using Matlab's **fminsearch** function. Because this unconstrained nonlinear optimization requires an initial guess, a method for selecting a valid initial guess was implemented. This method created a table of Cartesian tip errors by sampling the workspace using a uniform discretization of actuator values, calculating tip positions using these actuator values with the forward kinematics, and comparing these positions with the desired target position. The minimum error value in this table was then found, which corresponded to the "best" initial guess for D_1, D_2, and θ. The final actuator values were then calculated with **fminsearch** using these actuator values as initial guesses.

2.3 Deployment Sequence

To deploy the active cannula, an intuitive sequence using the actuator values obtained with the inverse kinematics was followed. First, the inner tube was rotated to θ. Both tubes and the USITT were then inserted together at the same speed until the base of the outer tube had reached D_1. Finally, the inner tube and the USITT were then inserted together until the inner tube had reached D_2.

3. CALIBRATION AND REGISTRATION

3.1 Ultrasound Calibration

There are many different methods used to calibrate free-hand ultrasound systems[19], and the method used was selected because it could be accomplished quickly and did not require the creation of a phantom. In order to relate ultrasound image coordinates to locations in three-dimensional space, the transformation between image coordinates and the optical tracking marker on the transducer handle must be determined. To estimate this transformation, the transducer was held in place and its pose recorded, while imaging in a 9.5 % ethanol solution (the speed of sound in this medium matches that expected in biological tissues, namely 1540 m/s[20]). The tip of an optically tracked probe was then inserted into the mixture and its coordinates were recorded. This procedure was repeated 25 times, a plane fit to the points, and the points projected into the plane. This process assumes that the US beam can be approximated as a plane and that the tip of the tracked probe can be positioned in it. This appears to be a reasonably accurate assumption, given that the average distance of the probe points to the plane fit to them was 1.29 ± 1.07 mm.

The tip of the tracked probe was then manually segmented in the US images. The ultrasound image points were then fit to the plane-projected probe points by point-based registration. The result of this registration is a homogenous transformation relating an US image pixel position to the coordinate frame of the transducer. In this process, 21 of the collected points were used to generate the calibration, and the remaining 4 were used to

provide an approximation of the calibration error. These points were transformed into world (optical tracker) coordinates using the calibrated transformation. These were then compared to the corresponding tracked point probe positions, resulting in a target registration error of 1.33 ± 0.98 mm.

3.2 Robot Calibration and Registration

To precisely position the tip of the ablator to a given point in the actuation unit coordinate frame, we require knowledge of the pose of the cannula's base frame with respect to the actuation unit coordinate frame. This information is expressed in the homogeneous transformation ${}^{C}T_{A}$ as shown in Figure 4.

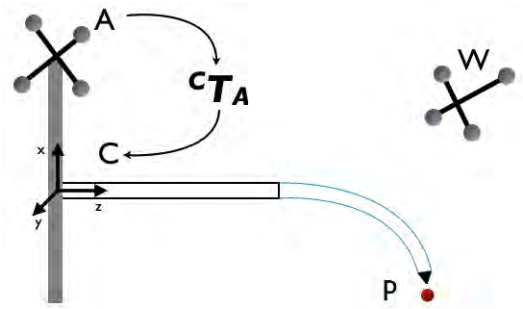

Figure 4. The homogeneous transformation ${}^{C}T_{A}$ relates the actuation unit frame A to the cannula frame C, which is needed to register the actuation space to the cannula space in order to accurately reach the target P. The world frame W is shown in space, however, the world frame in this paper was coincident with the cannula frame.

This transformation was determined using point-based registration[21]. We generated a set of 16 points in the cannula's base frame by discretizing the cannula's configuration space as shown in Table 1. The same ablator tip points can be measured in the world frame using an optically tracked probe. If the cannula's forward kinematic model were perfect, we could now apply point-based registration to determine the desired transformation.

However, we also wish to calibrate kinematic model parameters $\phi = \{\kappa_1, \kappa_2\}$ (see Figure 3) simultaneously with the registration. To accomplish this, we performed point-based registration on the two data sets at each step of an unconstrained nonlinear optimization. This optimization takes place over the model parameters ϕ, and is implemented using Matlab's `fminsearch` function. At each step, the cannula model point set is regenerated using the forward kinematic model with current model parameters, before the point-based registration is computed.

Table 1. Actuator values used for point-based registration.

n	Outer Tube (mm)	Inner Tube (mm)	Rotation (deg)
1	80	160	0, 90, 180, 270
2	80	120	0, 90, 180, 270
3	40	120	0, 90, 180, 270
4	40	80	0, 90, 180, 270

The registration and calibration procedure was used on 4 independent datasets. The average FRE without model parameter optimization was 1.19 mm and the average FRE after optimization was 1.09 mm. In the best case, which was then used for performing the actual targeting experiments, the FRE for the nominal model parameters was 0.94 mm. After applying the calibration algorithm, the FRE improved to 0.82 mm.

4. EXPERIMENTAL RESULTS

We performed targeting experiments to evaluate the accuracy of the system according to the workflow shown in Figure 5. The user (e.g. physician) selects a target in the ultrasound image. Using the registration methods described previously, this point is transformed into the robot's coordinate frame, and the robot's inverse kinematics algorithm is used to determine actuator positions. The robot is then deployed to these positions. To assess accuracy, a second image is collected in which the cannula tip is selected. The position of the tip of the cannula is compared to the initially selected desired image point.

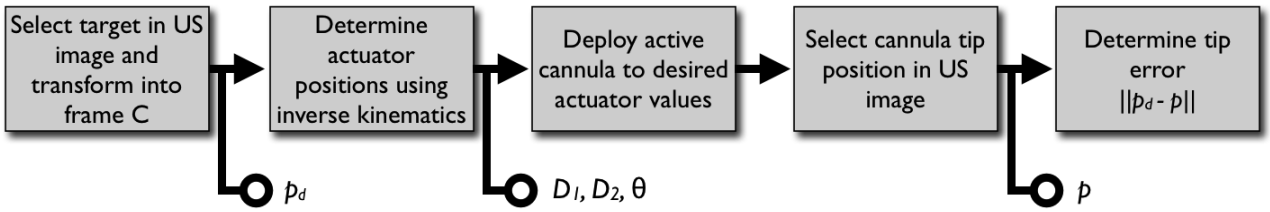

Figure 5. Workflow used for targeting experiments.

Three different insertion mediums were used in the experiments: a water-ethanol mixture (90:10) at room temperature that replicated the speed of ultrasound in liver tissue (1540 m/s), an artificial phantom made of Polyvinyl Chloride (M-F Manufacturing, TX), and an ex-vivo porcine liver.

4.1 Water Bath Experiment

To test the system described in this paper independent of a soft tissue medium, an aluminum cone was placed into a water-ethanol bath, to serve as the target (see Figure 6). For each insertion, the aluminum cone was placed at a different position in the bath. The cone tip was manually selected in the ultrasound image as the desired target, and the workflow illustrated in Figure 5 was implemented. The final cannula tip position was determined in the ultrasound image as shown in Figure 6b.

The cannula tip error in all targeting experiments was calculated as $||p_d - p||$. In the water-ethanol mixture, the average error for the water bath experiments was 1.25 mm with a standard deviation of 0.01 mm in 2 trials. It is noted that this error includes the tracking error of 0.35 mm as reported by NDI, ultrasound probe calibration error of 1.3 mm +/- 0.98 mm, and the active cannula calibration error due to unmodeled behavior such as friction, backlash, and misalignment.

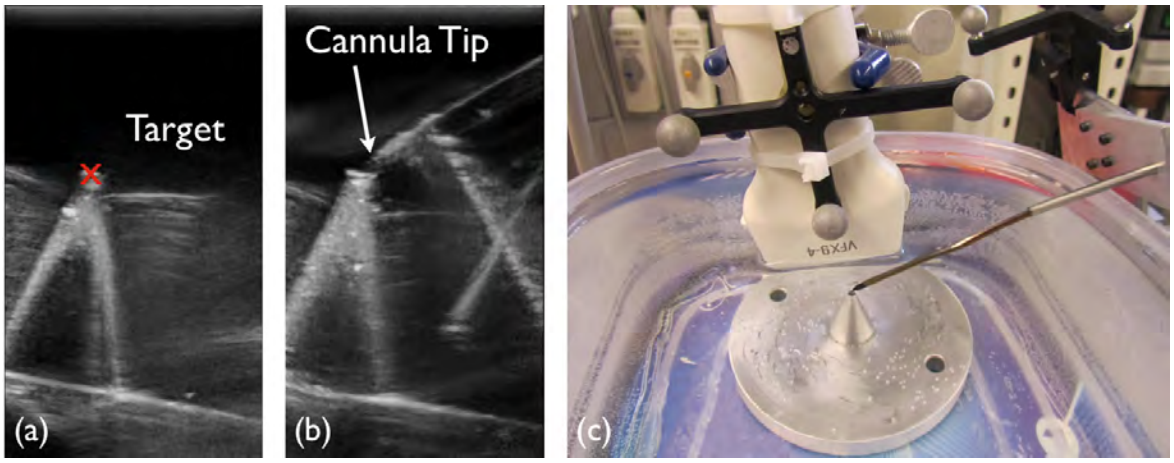

Figure 6. (a) Ultrasound image showing the selected target, i.e. the tip of the aluminum cone. (b) Cannula shown in ultrasound approaching the target. (c) Setup of water-ethanol targeting experiment with tracked ultrasound probe and cannula inserted.

4.2 Phantom Tissue Experiment

A second set of targeting experiments was performed in an artificial phantom made of Polyvinyl Chloride (M-F Manufacturing, TX). In order to create well-defined, identifiable targets in the ultrasound images, thin wooden dowels were inserted into the phantom at different locations as shown in Figure 7c. Each dowel cross section appears as a circular object in the ultrasound images (see Figure 7a). The dowels were manually selected as target positions. After the robot approached the target position, the cannula tip position was manually segmented in an ultrasound image as seen in Figure 7b.

This experiment was repeated five times with a different target location on each trial. The results of the experiment are summarized in Table 2. The average error for these experiments was 3.85 mm with a standard

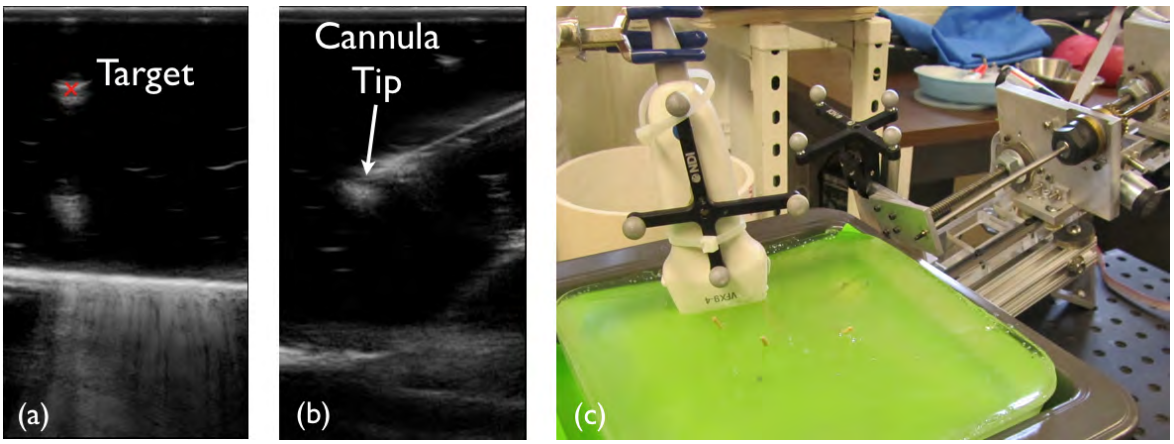

Figure 7. (a) Ultrasound image showing the selected target, i.e. the inserted dowel. (b) Cannula shown in ultrasound at the target. (c) Setup of phantom targeting experiment with dowel targets visible and cannula retracted.

deviation of 1.6 mm. The targeting error is higher than the water-ethanol experiments due to the cannula-phantom interaction forces and the fact that the Plastisol has a higher density than the water-ethanol mixtures. This resulted in a higher speed of sound, which caused some ultrasound image distortion. The ultrasound machine used was calibrated for a speed of sound of 1540 m/s, hence targets in Plastisol were reported as further away in the ultrasound image than they actually were.

Table 2. Phantom tissue targeting experiment results.

Run #	1	2	3	4	5
Tip Error (mm)	2.66	1.70	5.88	3.55	5.47

4.3 Ex Vivo Liver Experiment

In a third set of targeting experiments, ex vivo porcine liver was used as the insertion medium. A styrofoam container and plastic shrink-wrap held the sample in place. The cannula and ablator were introduced into the sample through a small hole in the side of the container. Figure 8 shows the experimental setup used. Targeting was performed using the same procedure described in the phantom and water-ethanol experiments above.

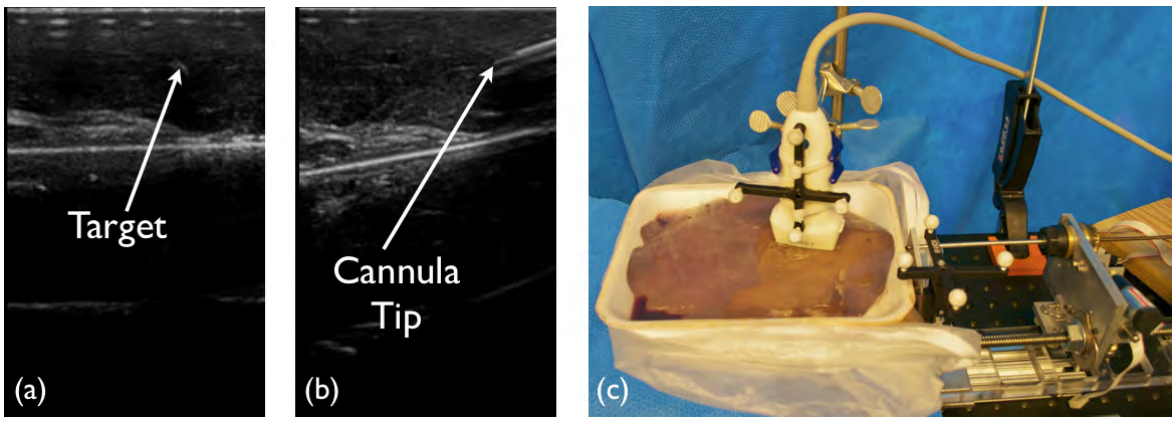

Figure 8. (a) Ultrasound image showing the selected target, i.e. the inserted dowel. (b) Cannula shown in the ultrasound image reaching the target. (c) Setup of ex-vivo porcine liver targeting experiment.

Five insertions were performed in ex vivo porcine liver with a separate target selected in each. The average error was 3.66 mm with a standard deviation of 0.23 mm. The results of each insertion can be seen in Table 3.

The improvement in targeting in ex-vivo liver can be attributed to the fact that the ultrasound machine was calibrated for use with liver.

Table 3. Ex-vivo liver targeting experiment results.

Run #	1	2	3	4	5
Tip Error (mm)	3.79	3.91	3.62	3.67	3.31

5. CONCLUSION AND FUTURE WORK

The active cannula robot enables a single insertion point with multi-site targeting for liver ablation. In addition to the ability to hit multiple targets, the maneuverability of the active cannula may allow physicians to steer around sensitive structures and reach inaccessible sites for ablation procedures. The experimental targeting results verify that the active cannula can be used under ultrasound guidance for targeting in soft tissue.

Moving forward, a system incorporating trackerless ultrasound[22], the USITT ablator, thermal monitoring with US[23], and the robotic active cannula actuation unit is envisioned. Trackerless ultrasound will remove the need for a clear line of sight between the probe and the camera system, allowing the surgeon more room to work in the operating room. US-based thermal monitoring will allow the physician to view the thermal lesion and ensure that the desired ablation zone is treated.

ACKNOWLEDGMENTS

This work was supported in part by National Science Foundation Grant IIS-1054331, in part by The National Institutes of Health under Grants R44 CA13416 and R21 EB011628, and in part by the National Institutes of HealthNational Institute for Neurological Disorders and Stroke under Grant R01 NS049251. Its contents are solely the responsibility of the authors and do not necessarily represent the official views of the NSF or NIH.

REFERENCES

[1] Taylor, R. H., "A Perspective on Medical Robotics," *Proceedings of the IEEE* **94**(9), 1652–1664 (2006).

[2] Cowan, N. J., Goldberg, K., Chirikjian, G. S., Fichtinger, G., Alterovitz, R., Reed, K. B., Kallem, V., Park, W., Misra, S., and Okamura, A. M., [*Robotic Needle Steering: Design, Modeling, Planning, and Image Guidance*], 557–582, Springer (2011).

[3] Boctor, E. M., Choti, M. A., Burdette, E. C., and Webster III, R. J., "Three-dimensional ultrasound-guided robotic needle placement: an experimental evaluation," *The International Journal of Medical Robotics Computer Assisted Surgery* **4**(2), 180–191 (2008).

[4] DiMaio, S. P. and Salcudean, S. E., "Needle insertion modeling and simulation," *IEEE Transactions on Robotics and Automation* **19**(5), 864–875 (2003).

[5] Glozman, D. and Shoham, M., "Image-Guided Robotic Flexible Needle Steering," *IEEE Transactions on Robotics* **23**(3), 459–467 (2007).

[6] Webster III, R. J., Kim, J. S., Cowan, N. J., Chirikjian, G. S., and Okamura, A. M., "Nonholonomic Modeling of Needle Steering," *The International Journal of Robotics Research* **25**(5-6), 509–525 (2006).

[7] Majewicz, A., Wedlick, T. R., Reed, K. B., and Okamura, A. M., "Evaluation of robotic needle steering in ex vivo tissue," *IEEE International Conference on Robotics and Automation* , 2068–2073 (2010).

[8] Okazawa, S., Ebrahimi, R., Chuang, J., Salcudean, S. E., and Rohling, R., "Hand-Held Steerable Needle Device," *IEEE/ASME Transactions on Mechatronics* **10**(3), 285–296 (2005).

[9] Webster III, R. J., Okamura, A., and Cowan, N., "Toward Active Cannulas: Miniature Snake-Like Surgical Robots," *IEEE/RSJ International Conference on Intelligent Robots and Systems* , 2857–2863 (Oct. 2006).

[10] Terayama, M., Furusho, J., and Monden, M., "Curved multi-tube device for path-error correction in a needle-insertion system," *The International Journal of Medical Robotics Computer Assisted Surgery* **3**(2), 125–134 (2007).

[11] Dupont, P. E., Lock, J., Itkowitz, B., and Butler, E., "Design and Control of Concentric-Tube Robots," *IEEE Transaction on Robotics* **26**(2), 209–225 (2010).

[12] Rucker, D. C., Webster III, R. J., Chirikjian, G. S., and Cowan, N. J., "Equilibrium Conformations of Concentric-tube Continuum Robots," *The International Journal of Robotics Research* **29**(10), 1263–1280 (2010).

[13] Kim, W. R., Gores, G. J., Benson, J. T., Therneau, T. M., and Melton, L. J., "Mortality and hospital utilization for hepatocellular carcinoma in the United States," *Gastroenterology* **129**(2), 486–493 (2005).

[14] McLoughlin, J. M., Jensen, E. H., and Malafa, M., "Resection of colorectal liver metastases: Current perspectives," *Cancer Control* **13**(1), 32–41 (2006).

[15] Choti, M. A., "Surgical management of hepatocellular carcinoma: resection and ablation," *Journal of Vascular and Interventional Radiology* **13**(9 Pt 2), S197–S203 (2002).

[16] Burdette, E. C., Rucker, D. C., Prakash, P., Diederich, C. J., Croom, J. M., Clarke, C., Stolka, P., Juang, T., Boctor, E. M., and Webster III, R. J., "The ACUSITT ultrasonic ablator: the first steerable needle with an integrated interventional tool," *Proceedings of SPIE Medical Imaging* (2010).

[17] Diederich, C. J., Stafford, R. J., Nau, W. H., Burdette, E. C., Price, R. E., and Hazle, J. D., "Transurethral ultrasound applicators with directional heating patterns for prostate thermal therapy: in vivo evaluation using magnetic resonance thermometry," *Medical Physics* **31**(2), 405–413 (2004).

[18] Nau, W. H., Diederich, C. J., and Burdette, E. C., "Evaluation of multielement catheter-cooled interstitial ultrasound applicators for high-temperature thermal therapy," *Medical Physics* **28**(7), 1525–1534 (2001).

[19] Mercier, L., Langø, T., Lindseth, F., and Collins, D. L., "A review of calibration techniques for freehand 3-D ultrasound systems," *Ultrasound in Medicine Biology* **31**(4), 449–471 (2005).

[20] Martin, K. and Spinks, D., "Measurement of the speed of sound in ethanol/water mixtures," *Ultrasound in Medicine Biology* **27**(2), 289–291 (2001).

[21] Fitzpatrick, J., Hill, D., and Maurer Jr., C., [*Image Registration*], 447–513, SPIE Press (2000).

[22] Boctor, E. M., Stolka, P., Kang, H.-J., Clarke, C., Rucker, C., Croom, J., Burdette, E. C., and Webster III, R. J., "Precisely shaped acoustic ablation of tumors utilizing steerable needle and 3D ultrasound image guidance," *Proceedings of SPIE Medical Imaging* (2010).

[23] Rivaz, H., Fleming, I., Assumpcao, L., Fichtinger, G., Hamper, U., Choti, M., Hager, G., and Boctor, E., "Ablation monitoring with elastography: 2D in-vivo and 3D ex-vivo studies," *Medical Image Computing and Computer-Assisted Intervention* **11**(Pt 2), 458–466 (2008).